Available online at www.sciencedirect.com
ScienceDirect
International Journal of Pharmaceutics 351 (2008) 271–281
INTERNATIONAL JOURNAL OF PHARMACEUTICS
www.elsevier.com/locate/ijpharm

Pharmaceutical nanotechnology

Electromagnetic interference in the permeability of saquinavir across the blood–brain barrier using nanoparticulate carriers

Yung-Chih Kuo *, Chan-Ying Kuo

Department of Chemical Engineering, National Chung Cheng University, Chia-Yi, Taiwan 62102, Republic of China

Received 2 July 2007; received in revised form 14 August 2007; accepted 18 September 2007
Available online 22 September 2007

Abstract

Transport of antiretroviral agents across the blood–brain barrier (BBB) is of key importance to the treatment for the acquired immunodeficiency syndrome (AIDS). In this study, impact of exposure to electromagnetic field (EMF) on the permeability of saquinavir (SQV) across BBB was investigated. The *in vitro* BBB model was based on human brain-microvascular endothelial cells (HBMEC), and the concentration of SQV in receiver chamber of the transport system was evaluated. Polybutylcyanoacrylate (PBCA), methylmethacrylate-sulfopropylmethacrylate (MMA-SPM), and solid lipid nanoparticle (SLN) were employed as carriers for the delivery systems. Cytotoxicity of SLN decreased as content of cacao butter increased. Power of 5 mV was apposite for the study on HBMEC without obvious apoptosis. Square wave produced greater permeability than sine and triangle waves. The carrier order on permeability of SQV across HBMEC monolayer under exposure to EMF was SLN > PBCA > MMA-SPM. Also, a larger frequency, modulation or depth of amplitude modulation (AM), or modulation or deviation of frequency modulation (FM) yielded a greater permeability. Besides, enhancement of permeability by AM wave was more significant than that by FM wave. Transport behavior of SQV across BBB was strongly influenced by the combination of nanoparticulate PBCA, MMA-SPM, and SLN with EMF exposure. This combination would be beneficial to the clinical application to the therapy of AIDS and other brain-related diseases.

Keywords: Blood–brain barrier; Electromagnetic field; Polybutylcyanoacrylate; Methylmethacrylate-sulfopropylmethacrylate; Solid lipid nanoparticle; Saquinavir

1. Introduction

Blood–brain barrier (BBB) is an important tissue site, providing a neurogenic environment for homeostasis of the central nervous system (CNS) against intense fluctuations in the level of substances in the circulatory system (Clark, 1999; Edwards, 2001). Brain-microvascular endothelial cells (BMEC) play a crucial role in the BBB characteristics. For example, tight junction (TJ) among BMEC is a key structure in avoiding dramatic influences of neurotransmitters and hormones on the cerebrum. Also, P-glycoprotein in BMEC membrane generates several essential pharmacological functions for drug carriage and expulsion (Gelperina et al., 2002).

Transport of anti-human immunodeficiency virus (HIV) agents across BBB is a prerequisite for the treatment of the acquired immunodeficiency syndrome (AIDS) (Glynn and Yazdanian, 1998) because HIV is replicated in the brain of HIV-infected individuals (Pang et al., 1990). Saquinavir (SQV) is a protease inhibitor for reducing enzymatic activity and inducing immature filial generation of HIV. That is, SQV medication generates noninfectious virus to obtain curative effect on the AIDS therapy. Although SQV is hydrophobic with log (octanol/buffer partition coefficient) of 4.51 and possesses high bioavailability via oral administration, the BBB permeability of SQV is very low (Lemberg et al., 2002; Li and Chan, 1999; Strazielle and Ghersi-Egea, 2005).

For drug delivery into CNS, pharmaceutical strategies, such as unfolding of TJ hiatus, utilization of prodrugs, and mediation by carrier systems, have been developed. Since pharmaceuticals are normally ionogenic through absorption or dissociation of protons in plasma, charged colloids become beneficial to the carrier-medicated delivery. Polybutylcyanoacrylate (PBCA) and methylmethacrylate-sulfopropylmethacrylate (MMA-SPM) were efficacious nanoparticle (NP) carriers for meliorating permeability of zidovudine and lamivudine across BBB (Kuo and Chen, 2006). Besides, concentrations of doxorubicin (Fundrao et al., 2000) and camptothecin (Yang et al., 1999) in rat brain tissue were obviously increased by

* Corresponding author. Tel.: +886 5 272 0411x33459; fax: +886 5 272 1206.
E-mail address: chmyck@ccu.edu.tw (Y.-C. Kuo).

0378-5173/$ – see front matter © 2007 Elsevier B.V. All rights reserved.
doi:10.1016/j.ijpharm.2007.09.020

entrapment in solid lipid nanoparticles (SLN). The three particulate formulations were capable of brain-targeted delivery and dosage reduction.

Exposure to electromagnetic field (EMF) could cause significant alteration in the BBB behavior. In a study on the transport of D-mannitol across BBB, it was observed that a higher power generally yielded larger permeability, and pulse wave was more effective in the permeability enhancement than continuous wave (Oscar and Hawkins, 1977). Also, intensity of sodium fluorescein in brain tissue exposed to EMF for 30 min was larger than that without EMF treatment (Williams et al., 1984a). Twofold increase in BBB permeability of sucrose was obtained after exposure to EMF of 1.8 GHz over 4 days (Schirmacher et al., 2000). For the thermal effect of EMF on BBB permeability, permeability enhancement was accompanied with an increase of 0.4 °C in brain tissue (Albert and Kerns, 1981). However, thermal effect of EMF might not be the predominant reason for permeability enhancement because the temperature increase was within the variation of 1 °C in daily rhythm. In a study on the penetration of horseradish peroxidase across BBB, horseradish peroxidase was observed in the outer zone of BMEC after exposure to EMF for 2 h, and regular transport was retrieved after termination of EMF for 1–2 h, indicating temporary alteration in BBB behavior by EMF exposure (Williams et al., 1984b).

In the present study, permeability of SQV across BBB under exposure to EMF was investigated *in vitro*. Here, BBB model was based on human BMEC (HBMEC), and SQV was incorporated with PBCA, MMA-SPM, and SLN. Effects of systematic parameters of EMF, including power, wave types, frequency, modulation and depth of amplitude modulation (AM) wave, and modulation and deviation of frequency modulation (FM) wave, were especially examined.

2. Materials and methods

2.1. Reagents and chemicals

Ammonim persulfate (APS), mannitol, Dulbecco's phosphate buffered saline (DPBS), L-α-phospatidylcholine (PC), cholesteryl hemisuccinate, taurocholate, D-trehalose, fluorescein isothiocyante (FITC)-conjugated dextrain, gelatin, trypsin–EDTA, rat-tail collagen, human fibronectin, 3-(4,5-dimethyl thiazol-2-yl)-2,5-diphenyl-tetrazolium bromide (MTT), anti-human von Willebrand factor VIII, anti-rabbit IgG with FITC conjugate, and [^{14}C]sucrose were purchased from Sigma (St. Louis, MO). Sulfopropyl methacrylate and docosanoic acid were obtained from Aldrich (Milwaukee, WI). Methyl methacrylate (MMA) and dextran 70,000 were purchased from Fluka Biochemika (Buchs, Switzerland). SQV was obtained from United States Pharmacopeial (Rockville, MD), butylcyanoacrylate (BCA) from Sicomet (Sichel Werk, Germany), polysorbate 80 from FisherScientific (Fair Lamn, NJ), acetonitrile from BDH (Poole, England), cacao butter (CB) from OCG Cacao (Whitinsville, MA), endothelial cell medium (ECM) from Biocompare (South San Francisco, CA), polycarbonate membrane from Millipore (Bedford, MA), Triton-X 100 from Acros (Geel, Belgium), methanol from Mallinckrodt Baker (Phillipsburg, NJ), and ultrapure water from Nanopure Infinity Ultrapure System of Barnstead (Dubuque, IA).

2.2. Preparation of SQV-incorporated carriers

Synthesis processes of PBCA and MMA-SPM nanoparticles and loading procedures of SQV were described previously (Kuo, 2005) with minor modifications. Briefly, BCA was polymerized in an acidic medium containing dextran 70,000 at 25 °C. MMA and SPM were copolymerized in the presence of APS at 78 °C over 24 h. PBCA and MMA-SPM suspensions were purified by centrifugation at 5100 × *g* for 10 min, filtrated through a filter, refrigerated at −80 °C in an ultra-low temperature freezer (Sanyo, Osaka, Japan) for 30 min, and lyophilized (Eyela, Tokyo, Japan) in the presence of 4% (w/v) mannitol at −80 °C over 36 h. 0.1% (w/v) SQV was mixed with 0.6% (w/v) lyophilized PBCA or MMA-SPM in DPBS. SQV was adsorbed onto PBCA and MMA-SPM in a baths-reciprocal shaker at 150 rpm and 37 °C for 3 h. The SQV-loaded polymers were stabilized by polysorbate 80 at 150 rpm and 37 °C for 30 min. The polysorbate 80-stabilized PBCA and MMA-SPM were treated by EMF with continuous electromagnetic wave of 5 mW and 915 MHz for 90 min. After ultracentrifugation (5415D, Eppendorf AG, Hamburg, Germany) at 11,500 × *g* for 1 h, loading efficiency was evaluated by high performance liquid chromatography (HPLC, Jasco, Tokyo, Japan) with a UV–vis spectrophotometer (UV-2075 Plus, Jasco, Tokyo, Japan) at 239 nm. Two high pressure pumps (PU-2080 Plus, Jasco, Tokyo, Japan) in series were applied to the mobile phase containing gradient of acetonitrile from 5 to 45% with a flow rate of 0.85 ml/min for 20 min. On the other hand, SQV-entrapped SLN was prepared by the method described previously (Kuo and Su, 2007) with minor modifications. Concisely, 7% (w/v) lipid, containing CB and docosanoic acid, SQV, 7% (w/v) PC, 3% (w/v) cholesteryl hemisuccinate, and 10% (w/v) taurocholate were mixed at 85 °C. The liquid was added drop by drop into ultrapure water at 3 °C under magnetic stirring for 15 min with lipid-to-water ratio of 1:10. SLN suspension was treated with continuous electromagnetic wave of 5 mW and 915 MHz for 90 min, filtrated and centrifuged at 14,000 × *g* for 30 min. Molecular SQV in supernatant was analyzed by HPLC followed by UV, and SLN pellet was resuspended with 2% (w/v) D-trehalose, refrigerated at −80 °C for 30 min and lyophilized. Entrapment efficiency (EE) of SQV was defined by EE = (total weight of SQV − weight of molecular SQV in supernatant)/total weight of SQV. For fluorescent carriers, FITC-conjugated dextrain were incorporated as stabilizer, loading agent, or entrapping substance.

Particle size distribution of SQV-incorporated carriers was obtained by a zetasizer 3000 HS_A with photo-correlation spectroscopy (Malvern, Worcs, UK). Infrared absorption spectra were analyzed by a Fourier-transform infrared spectrometer (FTIR, Shimadzu, Columbia, MD). Particle sizes of PBCA, MMA-SPM, and SLN were controlled, respectively, by reaction period, APS concentration, and stirring rate. The average diameters of PBCA, MMA-SPM, and SLN were, respectively,

92.4, 7.7, and 134.6 nm in the study on permeability under exposure to EMF. The continuous electromagnetic wave of 5 mW and 915 MHz for 90 min was selected because of low cellular injury, high permeability and reasonable period for medical treatment by EMF.

2.3. Characterization of HBMEC-based transport system exposed to EMF

Procedures for cultivation of HBMEC (Biocompare, South San Francisco, CA) were described previously (Kuo and Su, 2007) with minor modification. In brevity, HBMEC was unfrozen from liquid nitrogen in 37 °C water bath within 1 min and cultivated on culture dish coated by gelatin. During cultivation, ECM was replaced every 2 days. Over 6-day culture in a humidified CO_2 incubator (NuAire, Plymouth, MN) at 37 °C, HBMEC was detached by trypsin–EDTA for re-suspension. For estimation of viability under exposure to EMF, proliferated HBMEC of passage 6-16 was exposed to continuous electromagnetic wave of 915 MHz and various powers for 90 min. Deformation of HBMEC under exposure to EMF was observed by a phase contrast biological microscope (Motic, Richmond, BC) with both eyepiece and object lens at 10×, i.e., overall magnification of 100×. For *in vitro* BBB study, HBMEC supported on polycarbonate membrane was employed. First, HBMEC was seeded on polycarbonate membrane coated by rat-tail collagen and human fibronectin with surface density of 50 μg/cm^2 (Kuo and Chung, 2005). By seeding 6×10^4 cells/cm^2, confluent monolayer with tight junction was achieved over 14 day in the CO_2 incubator. Trans-endothelia electrical resistance (TEER) of HBMEC monolayer was determined by an electrical resistance system (Millipore, Bedford, MA) in ECM containing 0.25% (w/v) SLN for 90 min. Viability of HBMEC by treatment of 0.25% (w/v) SLN for 12 h and by stimulation of EMF was assayed through MTT using a UV–vis spectrophotometer (Bio-Tek Instruments, Winooski, VT) at 570 nm. For observation on carrier penetration, FITC-labeled nanoparticles were incubated with HBMEC on 18 mm cover slip for 90 min. Triton-X 100, anti-human von Willebrand factor VIII, and anti-rabbit IgG with FITC conjugate were applied to the stain of cytoplasm. Fluorescent images of the carrier uptake by HBMEC were obtained by argon laser with filter at 458 nm (excitation) and 488 nm (emission) under a phase contrast fluoromicroscope (Axioskop 2 plus, Zeiss, Munchen-Hallbergmoos, Germany) at 200×.

2.4. Electromagnetic interference in transport of SQV across HBMEC

The present BBB model based on HBMEC was described previously (Kuo and Su, 2007) with EMF involvement. The schematic representation of the transport system exposed to EMF is shown in Fig. 1. Briefly, jacket water at 37 °C was circulated in the exterior of donor and receiver chambers with magnetic stirring at the chamber bottoms for uniform distribution of carriers in the medium. The BBB model was placed at the bottom of a cylindrical copper coil with both axial length and diameter of 22 cm. Electromagnetic signals were transmitted to the copper coil from a radiofrequency synthesizer (Hameg, Mainhausen, Germany). EMF produced by magnetic stirring was negligible as compared with the applied EMF from the synthesizer. Fifty microliters of medium in receiver were sampled every 10 min, and the total volume was immediately compensated by 50 μL of fresh DPBS. Samples containing SLN carriers were dissolved in methanol. Ten milliliters of receiver fluid were ultracentrifuged at 11,500 × *g* for 2 h. Concentration of SQV in receiver was measured by the HPLC-UV system. [^{14}C]sucrose was used as a paracellular marker, and radioactivity in the transported samples was determined by a scintillation counter (Beckman, Palo Alto, CA). Permeability coefficient of SQV across HBMEC under exposure to EMF, P_{HBMEC}, was evaluated by $(1/P_{HBMEC}) = (1/P_e) - (1/P_m)$ and $P_i = (J/\Delta C) = V_r(dC_r/dt)/(A\Delta C)$, where i, P_e, P_m, J, ΔC, and V_r are, respectively, the permeability index (e or m), the permeability across HBMEC on polycarbonate membrane, the permeability across polycarbonate membrane, the flux from donor to receiver, the concentration difference between donor and receiver, and the receiver volume.

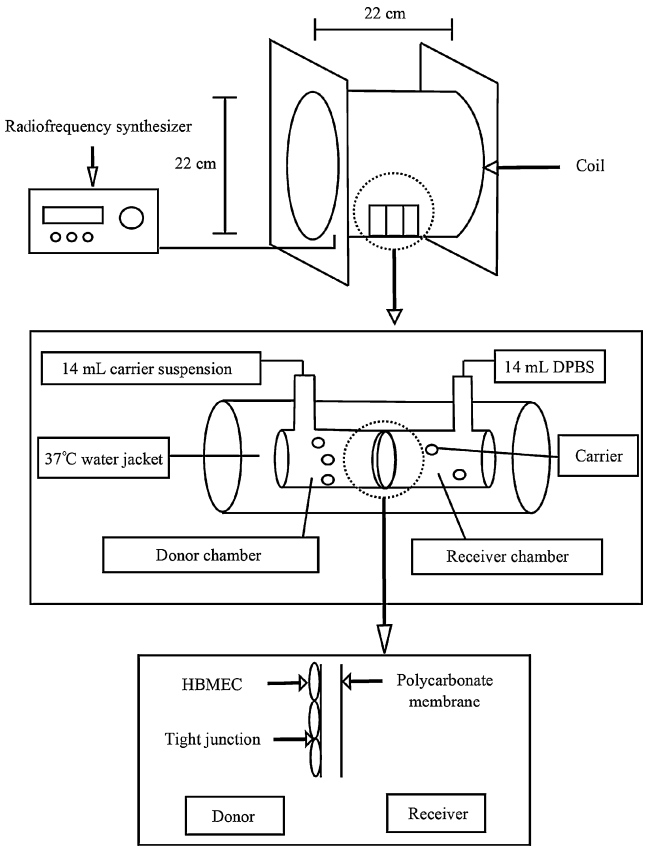

Fig. 1. Schematic illustration of the *in vitro* BBB transport system under exposure to EMF.

3. Results and discussion

3.1. Carrier size and entrapment efficiency of SQV

Fig. 2 shows the variation in carrier diameter and entrapment efficiency as functions of content of cacao butter, weight

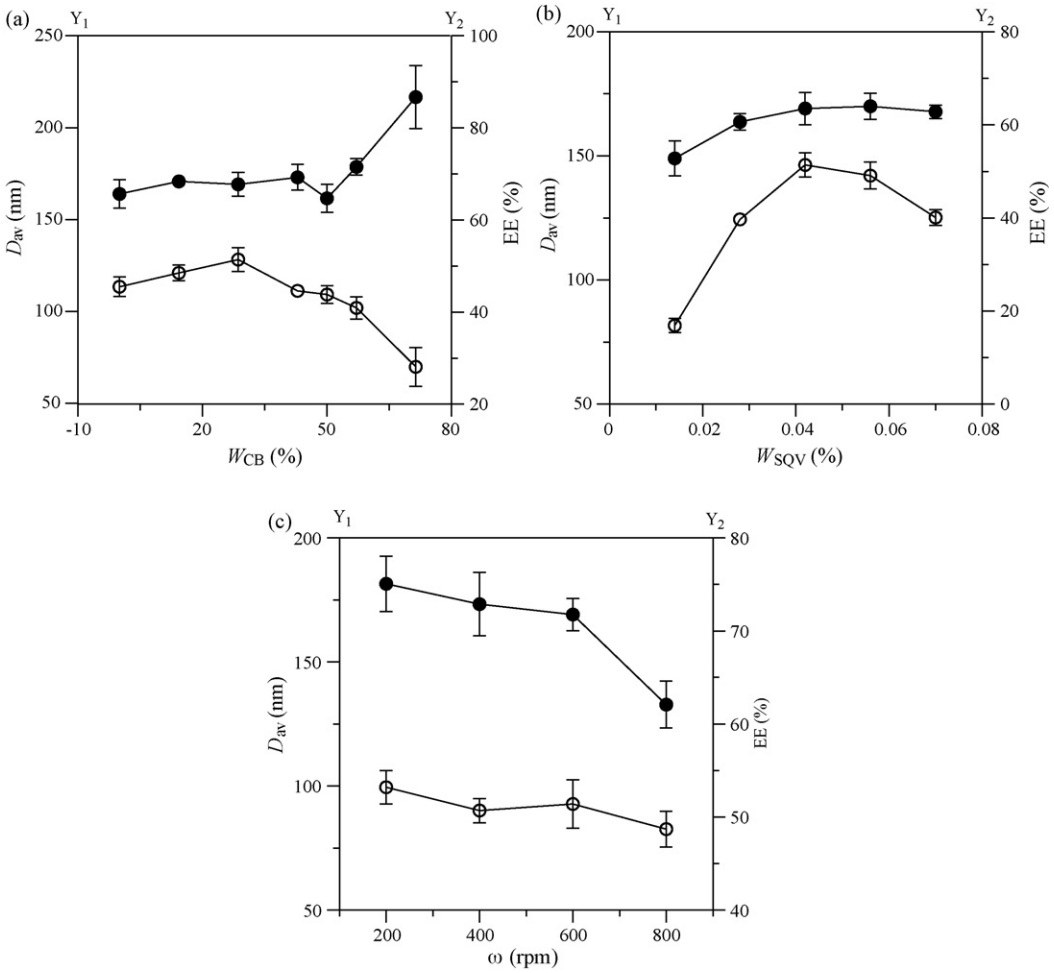

Fig. 2. Influence of the present drug-delivery-system parameters on average diameter, D_{av}, and entrapment efficiency, EE. Studied parameters were content of cacao butter, W_{CB}, in (a), weight percentage of SQV, W_{SQV}, in (b), and stirring rate, ω, in (c). Filled circles for D using Y_1 axis and empty circles for EE using Y_2 axis. Key: (a) W_{SQV} = 4.1% (3:73) and ω = 600 rpm, (b) W_{CB} = 28.6% (2:7) and ω = 600 rpm, and (c) W_{SQV} = 4.1% and W_{CB} = 28.6%.

percentage of SQV, and stirring rate. Here, content of cacao butter was the weight percentage of cacao butter in lipid. As revealed in Fig. 2(a), particle size increased with content of cacao butter when content of cacao butter was greater than 50%. However, an increase in content of cacao butter yielded a decrease in entrapment efficiency when content of cacao butter was greater than 28.6%. As suggested in Fig. 2(b), particle size and entrapment efficiency increased with weight percentage of SQV when weight percentage of SQV was less than 4.1%. The result about particle size was consistent with the literature report (Cavalli et al., 2000). As presented in Fig. 2(c), a high stirring rate caused a decrease in particle size. However, entrapment efficiency was not strongly affected by stirring rate.

Uniform size of carriers was beneficial to the control of incorporation and permeability of drugs because uniform size yielded same properties of every individual particle, rendering identical drug delivery from each carrier to avoid abrupt release. The present formulations fulfilled this requirement for carrier size (Kuo, 2005). For the entrapment of SQV by cacao butter/docosanoic acid SLN, the ingredients of cacao butter played an import role. Note that cacao butter was composed of 24.4–26.2% palmitic acid, 34.4–35.4% stearic acid, 37.7–38.1% oleic acid, and 2.1% linoleic acid (Liend et al., 1997). Docosanoic, palmitic, and stearic acids were single-bond structure; oleic acid possessed *trans*-double bond; and linoleic acid possessed *cis*-double bond. Single and *trans*-double bonds might form more compact configuration than *cis*-double bond. Hence, when content of cacao butter was greater than 50%, the particle size increased with content of cacao butter, as indicated in Fig. 2(a). Since oleic acid was a minor ingredient in cacao butter, when content of cacao butter was less than 50%, little effect of content of cacao butter on the SLN size was observed (Quintanar-Guerrero et al., 2005). Besides, linoleic acid was not beneficial to the entrapment of SQV. Thus, entrapment efficiency decreased as content of cacao butter increased, in general. For the influence of drug content, when weight percentage of SQV was less than 4.1%, the dissolved amount of SQV in water and lipids increased with weight percentage of SQV. When weight percentage of SQV was greater than 4.1%, the dissolved amount of SQV in lipid core reached saturation although dissolved amount of SQV in water might still increase. Hence, entrapment efficiency exhibited a maximum at weight percentage of SQV = 4.1%, as

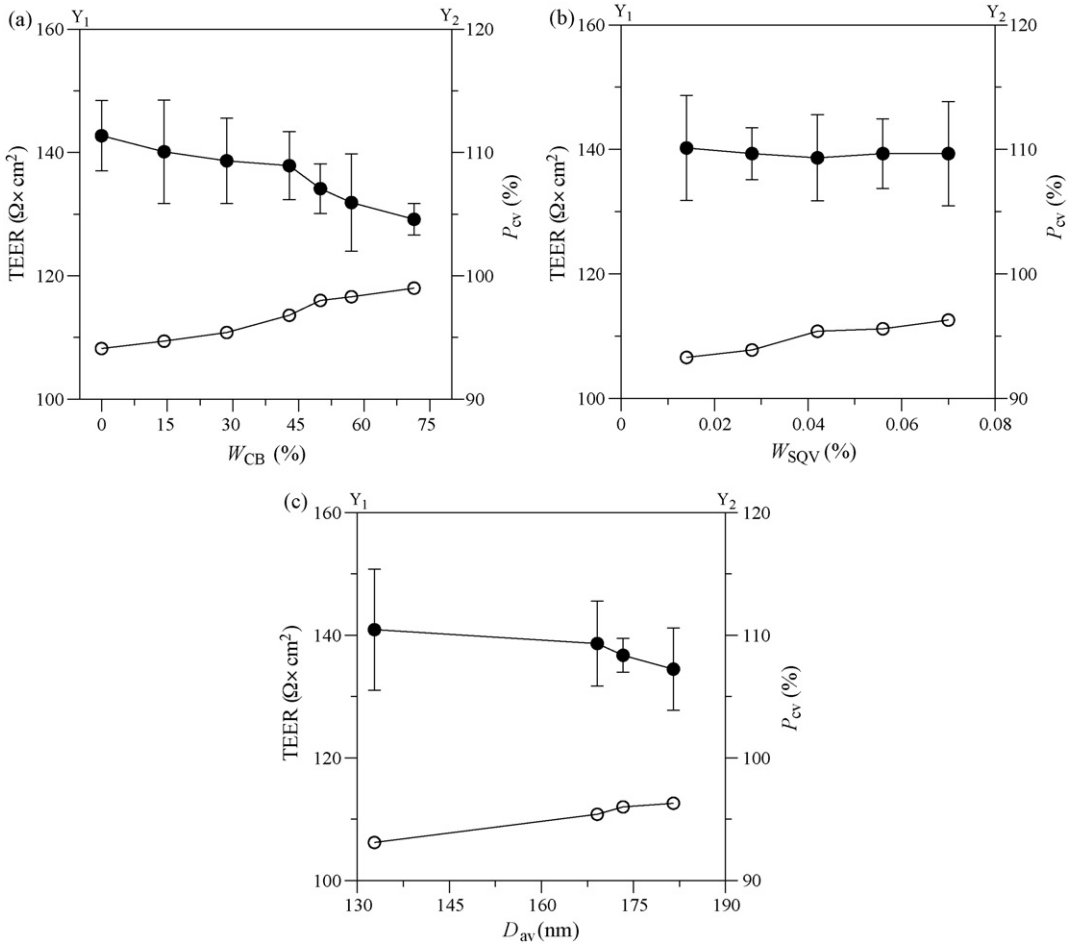

Fig. 3. Influence of the present drug-delivery-system parameters on transendothelial electrical resistance, TEER, and cell viability, P_{CV}. Studied parameters were content of cacao butter, W_{CB}, in (a), weight percentage of SQV, W_{SQV}, in (b), and average diameter, D_{av}, corresponding to stirring rate in (c). Filled circles for TEER using Y_1 axis and empty circles for P_{CV} using Y_2 axis. Key: same as Fig. 2.

shown in Fig. 2(b). For the effect of stirring rate, a high stirring rate represented a large shear stress. The larger the shear stresses on microemulsion drops dispersed in cold water, the larger the force to break up the drops, forming smaller SLN.

3.2. Cell viability and TEER of HBMEC monolayer

Fig. 3 presents the variation in TEER and cell viability as functions of content of cacao butter, weight percentage of SQV, and carrier diameter. As displayed in Fig. 3(a), a greater content of cacao butter led to a lower TEER and higher cell viability. As suggested in Fig. 3(b), TEER almost remained at a constant as weight percentage of SQV varied; however, an increase in weight percentage of SQV caused an increase in cell viability. A larger carrier diameter yielded a lower TEER and higher cell viability.

Cytotoxicity of drug carriers derived mainly from the following three mechanisms: the inflammatory mediators secreted after particulate stimulation, the temporary toxicity by particle attachment on cell membrane, and degraded products of carriers. Since small particle yielded frequent contact with cells, small carriers normally generated high toxicity (Kuo and Chung, 2005). On the other hand, confluent monolayer was usually determined by TEER. Endothelial monolayer cultivated from different animal source would display different TEER. The present HBMEC monolayer exhibited TEER of ca. 150 Ω cm^2. Since permeability of SLN was relatively high, slight TEER decrease were observed. For the effect of content of cacao butter, cellular viability increased with content of cacao butter because cacao butter was highly biocompatible and an increase in the content of cacao butter yielded a larger SLN. TEER was reduced by uptake of SLN because the negatively charged SLN would increase the electrical current of the monolayer. This was consistent with the observation that TEER was reduced by uptake of charged 1-palmitoyl-2-hydroxy-*sn*-glycero-3-phosphocholine particles (Huang et al., 2005). Since surface charge of SLN increased with content of cacao butter, uptake of SLN with high content of cacao butter caused a large reduction in TEER, as revealed in Fig. 3(a). It could also be concluded that a reduction in TEER resulted from electrostatic properties of SLN, not from HBMEC death. For the effect of weight percentage of SQV, drug dose was not the key reason for cell viability. It was because 0.32 μg/mL of SQV was almost harmless to cells (Molla et al., 2002), and the highest SQV con-

centration employed in the present study was 0.3 μg/mL. The main reason for cell viability was particle size. Smaller carriers fabricated at lower weight percentage of SQV resulted in lower cell viability. Besides, as revealed in Fig. 3(b), TEER was only slightly influenced by weight percentage of SQV because SQV was entrapped inside lipid core.

3.3. SQV incorporation, HBMEC viability, and carrier uptake under exposure to EMF

Fig. 4 shows the FTIR spectra of the carrier systems. The main functional groups of SQV were C–N, N–H, C–O, and C=O, and those of PBCA were C≡N, C–O, and C=O, as revealed in spectra (a) and (b). As indicated in spectra (c) and (d), the main functional groups of MMA-SPM were S–O, S=O, C=C, C–O, and C=O. The main functional groups of SLN were C=C, O–H, C–O, and C=O, as exhibited in spectra (e) and (f). Transmittances of C–N and N–H became slightly intense after electromagnetic treatment, implying that SQV could be successfully incorporated with carriers under exposure to EMF.

Fig. 5 displays the morphology of HBMEC under electromagnetic influence. As exhibited in Fig. 5(a), ellipsoidal HBMEC was commonly observed. Nuclei became apparent under power of 5 mW, as shown in Fig. 5(b). Under 10 mW, cellular deformation occurred, and bright vacuoles denoted cell death (apoptosis), as presented in Fig. 5(c). Obviously cellular shrinkage and irregular vacuoles were observed under 20 mW, as presented in Fig. 5(d). Table 1 also lists the cell viability under exposure to EMF of various powers. As shown in this table, the stronger the power, the lower the cell viability, which

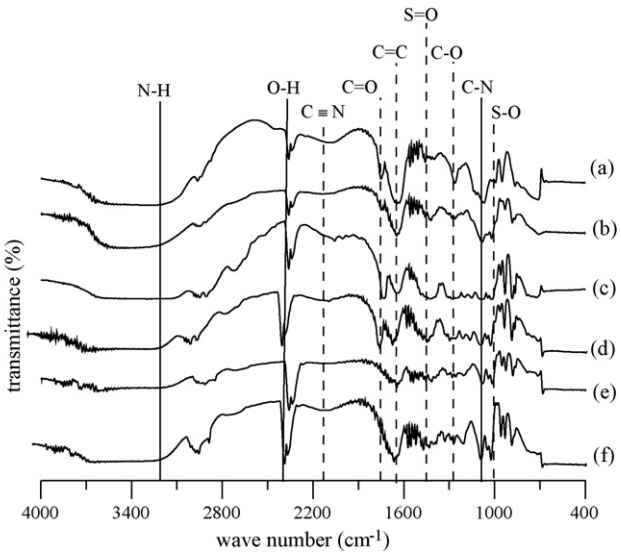

Fig. 4. FTIR spectra of the carrier systems. (a) PBCA, (b) PBCA with EMF exposure, (c) MMA-SPM, (d) MMA-SPM with EMF exposure, (e) SLN, and (f) SLN with EMF exposure. Key: EMF exposure was the application of continuous electromagnetic wave of 5 mW and 915 MHz for 90 min.

was consistent with Fig. 5. In a study on apoptosis induced by radiofrequency radiation, cell death under strong electromagnetic power might derive from the damage to DNA, and the range of death rate was 5–20% (Markkanen et al., 2004). Also, viability of T-lymphoblastoid leukemia CCRF-CEM cells reduced 19% under 13 mW and 915 MHz for 2 h (Sommerfeld et al., 1997). Since power of 5 mW produced low cell injury and death, this

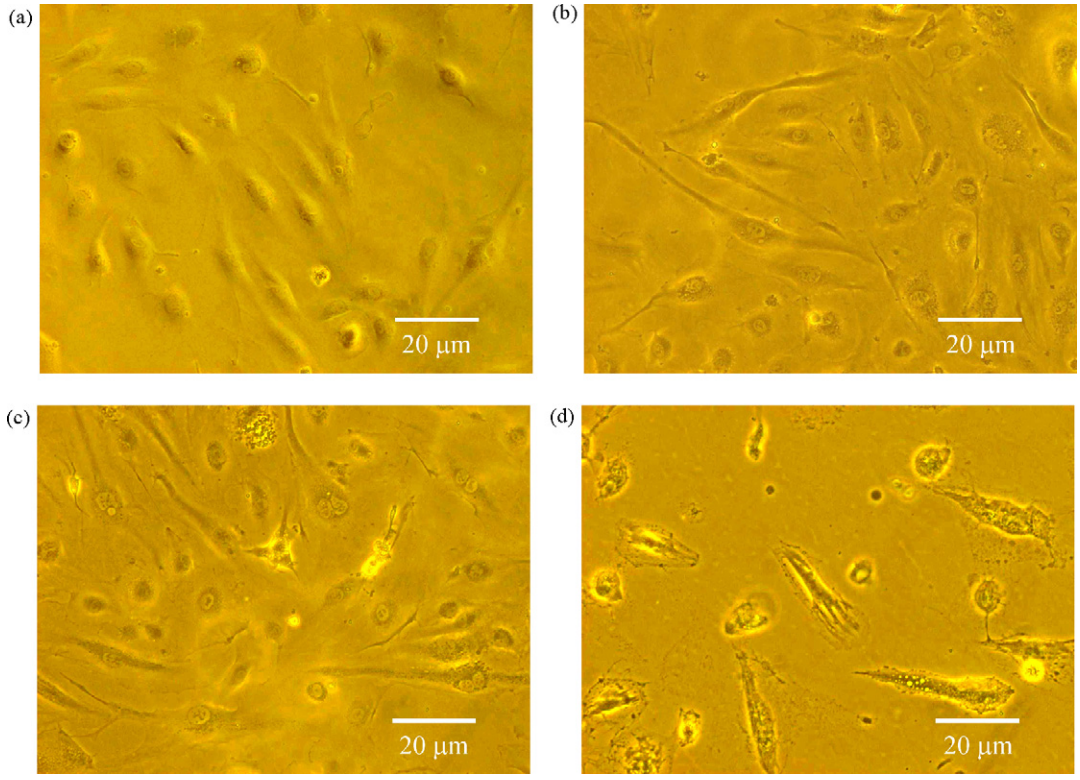

Fig. 5. Images of HBMEC exposed to continuous electromagnetic wave of 915 MHz for 90 min. (a) No EMF, (b) 5 mW, (c) 10 mW, and (d) 20 mW.

Table 1
Cell viability treated by continuous electromagnetic wave of 915 MHz for 90 min

Power (mW)	Cell viability (%)
5	95.32 ± 2.59
10	91.25 ± 2.42
20	82.15 ± 4.91

magnitude of electromagnetic power was appropriate for the following study on HBMEC.

Fig. 6 exhibits images for uptake of the three drug carriers by HBMEC. As shown in Fig. 6(a, c, and e), PBCA, MMA-SPM, and SLN could be recognized and absorbed by HBMEC. The corresponding images under exposure to EMF were presented in Fig. 6(b, d, and f). Bright green spots were the carriers. The amount of spots in Fig. 6(a) was close to that in Fig. 6(c), where SLN even penetrated into the nucleus. The amount of spots in Fig. 6(b) was less than that in Fig. 6(a and c). Moreover, for a fixed carrier, exposure to EMF increased the amount of spots, suggesting that electromagnetic wave was beneficial to the uptake of carriers by HBMEC.

MMA-SPM possessed comparatively low ability to penetrate HBMEC because high negative charge existed in MMA-SPM (Kuo and Lin, 2006). Moreover, MMA-SPM was a hydrophilic nanoparticle (Kuo, 2005) and hydrophobic substances were advantageous to the BBB transport (Krogh, 1946). For positively charged PBCA, BBB permeability was high due to the electrostatic effects (Kuo and Su, 2007). For the most efficient carrier, SLN yielded the highest permeability coefficient among the three colloidal particles. This was mainly because phospatidylcholine on the external surface of SLN could enhance the carrier penetration through membrane and nucleus of HBMEC, as evi-

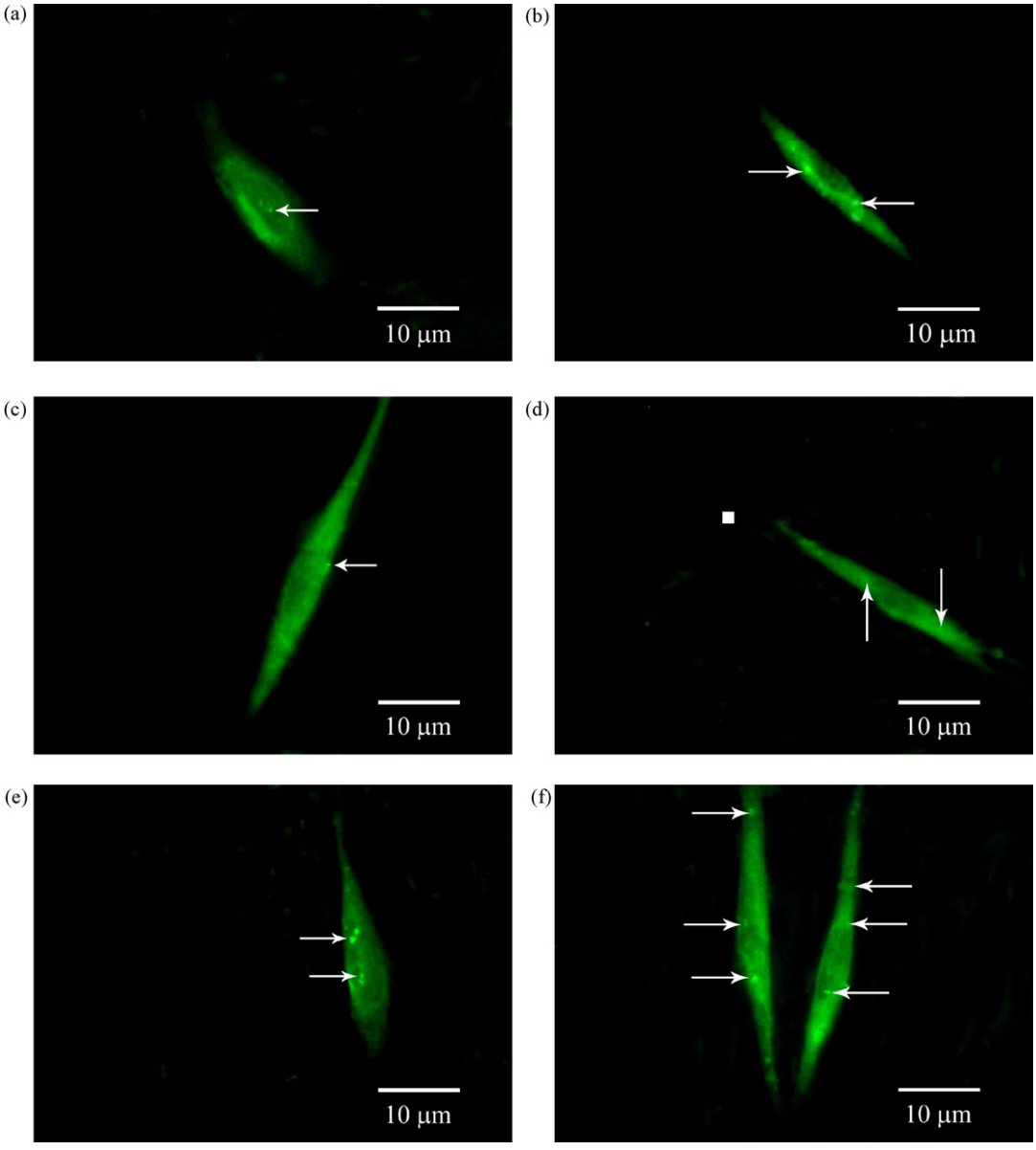

Fig. 6. Fluorescent images of the uptake of carriers by HBMEC. (a) PBCA, (b) PBCA with EMF exposure, (c) MMA-SPM, (d) MMA-SPM with EMF exposure, (e) SLN, and (f) SLN with EMF exposure. Arrows indicate the carriers. Key: same as Fig. 4.

denced in Fig. 6(e and f). Also, the zeta potential of the present SLN was −18 mV, implying that the negative electricity on SLN was relatively weak.

3.4. Electromagnetic interference in permeability of SQV across HBMEC

Fig. 7 presents the variation in permeability coefficient of SQV across HBMEC monolayer as a function of carrier diameter and continuous electromagnetic frequency. As shown in Fig. 7(a), permeability coefficient decreased as carrier diameter increased. The main reason was that a larger particle caused a greater mass-transfer resistance. Note that in the present study, permeability coefficient of molecular SQV was

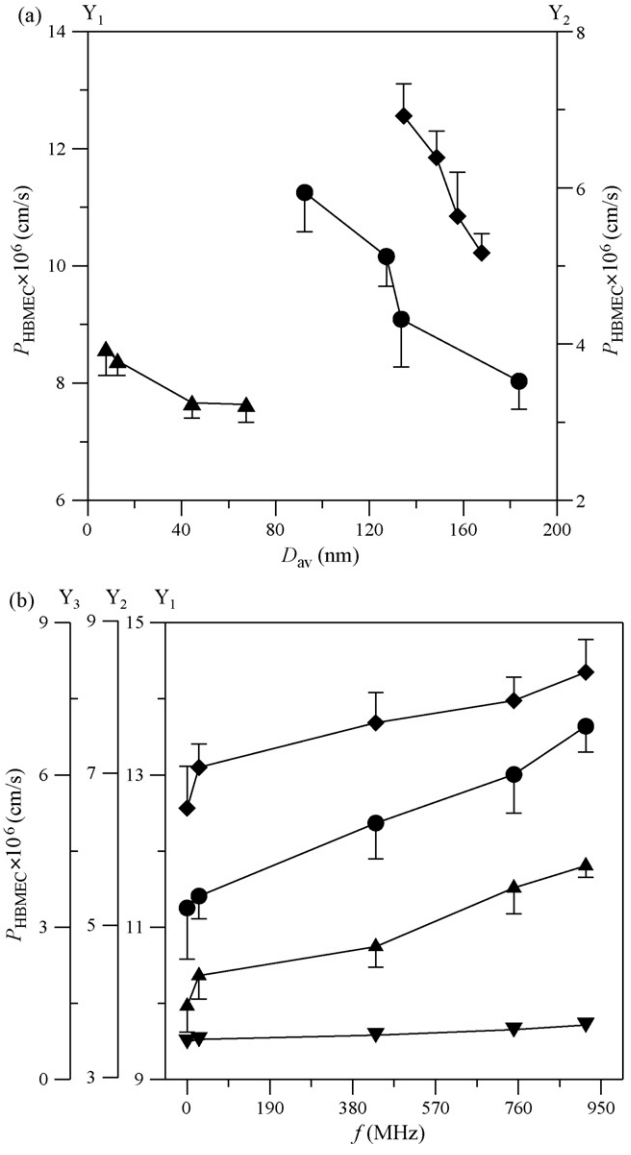

Fig. 7. Permeability coefficient of SQV across HBMEC monolayer, P_{HBMEC}, using PBCA, MMA-SPM, and SLN. (a) Influence of average diameter, D_{av}, and (b) influence of continuous electromagnetic frequency, f. In (b), EMF of 5 mW was applied. Key: diamonds for SLN using Y_1 axis, circles for PBCA using Y_1 axis, triangles for MMA-SPM using Y_2 axis, reverse triangles for molecular SQV using Y_3 axis.

Table 2
Permeability coefficient of SQV across HBMEC monolayer under exposure to EMF[a]

	Sine wave	Square wave	Triangle wave
AM[b]			
Molecular SQV	1.16 ± 0.10	1.25 ± 0.07	1.14 ± 0.08
PBCA[c]	15.42 ± 0.73	16.15 ± 0.92	15.39 ± 0.84
MMA-SPM[c]	6.91 ± 0.35	7.51 ± 0.44	6.69 ± 0.37
SLN[c]	15.63 ± 0.86	16.19 ± 0.97	15.54 ± 1.21
FM[d]			
Molecular SQV	1.18 ± 0.12	1.22 ± 0.09	–
PBCA[c]	14.32 ± 0.76	14.93 ± 0.58	–
MMA-SPM[c]	6.63 ± 0.29	7.15 ± 0.51	–
SLN[c]	14.75 ± 0.89	15.23 ± 0.61	–

[a] 5 mW and 915 MHz.
[b] Modulation: 20 MHz and depth: 100%.
[c] SQV incorporated carriers.
[d] Modulation: 20 MHz and deviation: 400 kHz.

0.746×10^{-6} cm/s. As displayed in Fig. 7(b), exposure to EMF produced enhancement effect on permeability coefficient of molecular and carrier-incorporated SQV. This was consistent with the literature result (Schirmacher et al., 2000). The enhancement effect for charged carriers was greater than that for molecular SQV. Besides, a higher frequency yielded a larger permeability coefficient. Nine hundred fifteen megahertz led to the largest permeability coefficient in the present study. For carrier species, permeability coefficient was on the order of SLN > PBCA > MMA-SPM. Table 2 lists permeability coefficient of the present formulations across HBMEC under exposure to EMF of various wave types. As revealed in this table, permeability coefficient under sine and triangle waves was comparable. Square wave produced the largest permeability among the three waves. Fig. 8 shows the effect of modulation and depth of AM-electromagnetic wave on permeability coefficient of SQV across HBMEC monolayer. As indicated in Fig. 8, an increase in modulation and depth caused an apparent increase in permeability coefficient of the carrier-mediated systems. Note that, molecular SQV without incorporation with carrier or surfactant was used as control groups, and an increase in modulation and depth resulted in a slight increase in permeability coefficient of molecular SQV. This was because surface charge on the three carriers was higher than charge of molecular drug. Fig. 9 presents the variation in permeability coefficient of SQV across HBMEC monolayer exposed to EMF of FM as a function of modulation and deviation. As revealed in Fig. 9, an increase in modulation and deviation also yielded an obvious increase in permeability coefficient of the carrier-mediated systems. For molecular SQV, an increase in modulation and deviation resulted in a slight increase in permeability coefficient. The order on permeability coefficient of SQV under both AM and FM waves followed SLN > PBCA > MMA-SPM.

Absorption of electromagnetic wave by tissue could be expressed by (Gabriel et al., 1996)

$$\mathrm{SAR} = \sigma \frac{|E|^2}{\rho}$$

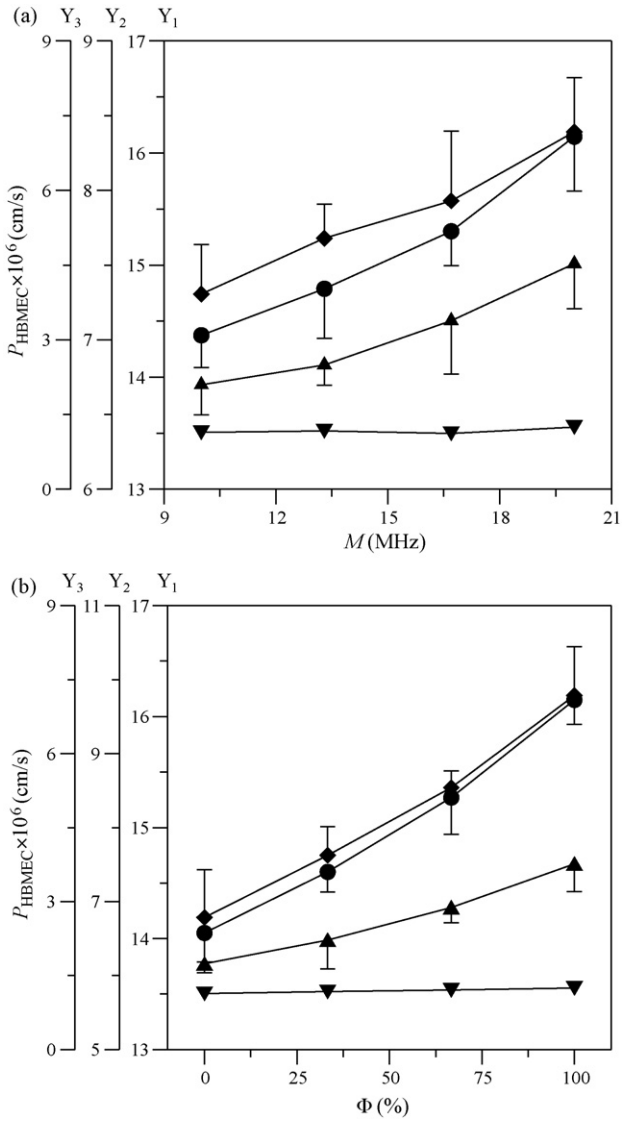

Fig. 8. Permeability coefficient of SQV across HBMEC monolayer, P_{HBMEC}, using PBCA, MMA-SPM, and SLN under exposure to EMF with amplitude modulation. (a) Influence of modulation, M, and $\Phi = 100\%$ and (b) influence of depth, Φ, and $M = 20$ MHz. Key: same as Fig. 7. Key 1: square wave of 5 mW and 915 MHz was applied.

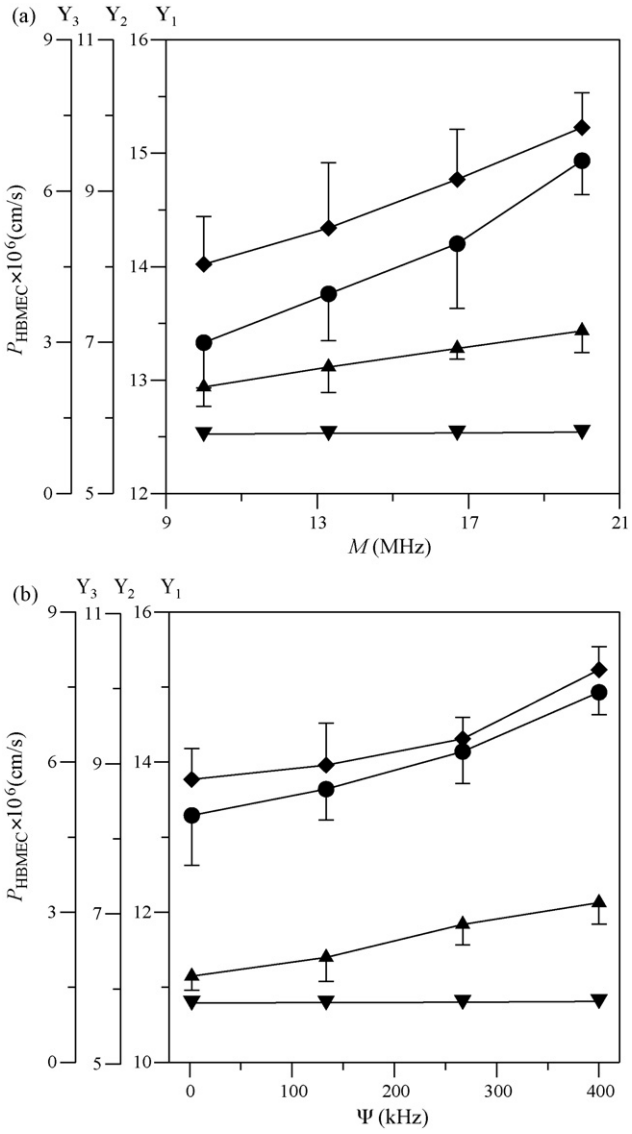

Fig. 9. Permeability coefficient of SQV across HBMEC monolayer, P_{HBMEC}, using PBCA, MMA-SPM, and SLN under exposure to EMF with frequency modulation. (a) Influence of modulation, M, and $\Psi = 400$ kHz and (b) influence of deviation, Ψ, and $M = 20$ MHz. Key: same as Fig. 7. Key 1: same as Fig. 8.

where SAR, σ, $|E|$, and ρ were, respectively, the specific absorption rate of tissue exposed to EMF, the electric conductivity, the magnitude of EMF, and the tissue density. It has been concluded that penetration across BBB increased as SAR increased (Salford et al., 1994). For the case of constant $|E|$ and ρ, an increase in SAR was resulted from an increase in σ. For human brain tissue, an increase in electromagnetic frequency yielded an increase in σ (Gabriel et al., 1996). It was also observed that an increase in electromagnetic frequency caused an increase in σ for Chinese hamster V79 cells (Bonincontro and Mariutti, 1988). Hence, a higher electromagnetic frequency produced a larger SAR, leading to a greater permeability coefficient. Furthermore, the function of wave type could be distinguished as followed. The mathematical descriptions of square, sine and triangle waves were, respectively, $f(t) = (4A/\pi)(\sin\omega t + (1/3)\sin 3\omega t + (1/5)\sin 5\omega t + \cdots)$, $f(t) = (4A/\pi)\sin\omega t$, and $f(t) = (8A/\pi^2)(\sin\omega t - (1/9)\sin 3\omega t + (1/25)\sin 5\omega t - \cdots)$. In these expressions, $\omega = 2\pi/T$, A, t, and T were the frequency, the amplitude, the time, and the period, respectively. By integrating these functions in one period, the power of square wave was the same as the direct current with amplitude of $4A/\pi$. Also, the power of sine and triangle waves was ca. 0.7 times the power of square wave. Hence, square wave generated the strongest $|E|$ and SAR among the three waves, yielding the largest permeability coefficient. Besides, electrical conductivity could also explain the effect of modulation on permeability of SQV. It was observed that for avian brain tissue under AM wave, σ at modulation of 16 Hz was 1.2 times that of 3 Hz (Albert et al., 1987). For human brain, σ also increased as FM modulation increased from 9

to 16 Hz (Blackman et al., 1979). Thus, a larger modulation induced greater permeability. Also, σ at depth of 50% was larger than that of 0% for AM wave with modulation of 16 Hz (Albert et al., 1987); and σ increased as deviation increased for FM wave with modulation of 16 Hz (Blackman et al., 1979). Hence, an increase in depth or deviation caused an increase in permeability. Moreover, comparing AM with FM, influence of AM modulation on permeability of SQV across HBMEC was stronger than that of FM modulation. The rationale of this result was interpreted below. In an investigation on murine L929 cell, ornithine decarboxylase (ODC) was activated by AM wave at 845 MHz; however, the activity of ODC was not affected by FM wave at 845 MHz (Peneafiel et al., 1993). ODC synthesized polyamines, which promoted the permeability of superoxide dismutase across animal cell membrane (Poduslo and Curran, 1996). Thus, AM was more influential to the penetration across HBMEC than FM.

4. Conclusions

Transport of SQV across *in vitro* BBB under exposure to EMF was investigated. Here, SQV was incorporated with nanoparticulate carriers including PBCA, MMA-SPM, and SLN, and the BBB model was based on HBMEC. Experimental results revealed that a high power of EMF caused apoptosis of HBMEC. For penetration across HBMEC monolayer, permeability of SQV was significantly enhanced by incorporation with the three carriers. Also, an apparent increase in permeability coefficient of SQV incorporated with the three carriers was resulted from an increase in continuous electromagnetic frequency, modulation or depth of AM wave, or modulation or deviation of FM wave.

Acknowledgment

This work is supported by the National Science Council of the Republic of China.

References

Albert, E.N., Slaby, F., Roche, J., Loftus, J., 1987. Effect of amplitude modulated 147 MHz radiofrequency radiation on calcium ion efflux from avian brain tissue. Radiat. Res. 109, 19–27.

Albert, E.N., Kerns, J.M., 1981. Reversible microwave effects on the blood–brain barrier. Brain Res. 230, 153–164.

Blackman, C.F., Elder, J.A., Weil, C.M., Benane, S.G., Eichinger, D.C., House, D.E., 1979. Induction of calcium-ion efflux from brain tissue by radiofrequency radiation: effects of modulation frequency and field strength. Radio Sci. 14, 93–98.

Bonincontro, A., Mariutti, G., 1988. Influence of hypertheria, pH and culturing conditions on the electrical parameters of Chinese hamster V79 cells. Phys. Med. Biol. 33, 557–568.

Cavalli, R., Caputo, O., Gasco, M.R., 2000. Preparation and characterization of solid lipid nanospheres containing paclitaxel. Eur. J. Pharm. Sci. 10, 305–309.

Clark, D.E., 1999. Rapid calculation of polar molecular surface area and its application to the prediction of transport phenomena. 2. Prediction of blood–brain barrier penetration. J. Pharm. Sci. 88, 815–821.

Edwards, R.H., 2001. Drug delivery via the blood–brain barrier. Nat. Neurosci. 4, 221–222.

Fundrao, A., Cavalli, R., Bargoni, A., Vighetto, D., Zara, G.P., Gasco, M.R., 2000. Non-stealth and solid lipid nanoparticles (SLN) carrying doxorubicin: pharmacokinetics and tissue distribution after i.v. administration to rats. Pharm. Res. 42, 337–343.

Gabriel, S., Lau, R.W., Gabriel, C., 1996. The dielectric properties of biological tissues: II. Measurements in the frequency range 10 Hz to 20 GHz. Phys. Med. Biol. 41, 2251–2269.

Gelperina, S.E., Khalansky, A.S., Skidan, I.N., Smirnova, Z.S., Bobruskin, A.I., Severin, S.E., Turowski, B., Zanella, F.E., Kreuter, J., 2002. Toxicological studies of doxorubicin bound to polysorbate 80-coated poly(butyl cyanoacrylate) naoparticles in healthy rats and rats with intracranial glioblastoma. Toxicol. Lett. 126, 131–141.

Glynn, S.L., Yazdanian, M., 1998. In vitro blood–brain barrier permeability of nevirapine compared to other HIV antiretroviral agents. J. Pharm. Sci. 87, 306–310.

Huang, F., Subbaiah, P.V., Holian, O., Zhang, J., Johnson, A., Gertzberg, N., Lum, H., 2005. Lysophosphatidylcholine increases endothelial permeability: role of PKCα and RhoA cross talk. Am. J. Physiol. Lung Cell Mol. Physiol. 289, 176–185.

Krogh, A., 1946. The active and passive exchanges of inorganic ions though the surfaces of living cells and though living membranes generally. Proc. Roy. Soc. Lond. B 133, 140–200.

Kuo, Y.C., Su, F.L., 2007. Transport of stavudine, delavirdine, and saquinavir across the blood–brain barrier by polybutylcyanoacrylate, methylmethacrylate-sulfopropylmethacrylate, and solid lipid nanoparticles. Int. J. Pharm. 340, 143–452.

Kuo, Y.C., Chen, H.H., 2006. Effect of nanoparticulate polybutylcyanoacrylate and methylmethacrylate-sulfopropylmethacrylate on the permeability of zidovudine and lamivudine across the in vitro blood–brain barrier. Int. J. Pharm. 327, 160–169.

Kuo, Y.C., Lin, T.W., 2006. Electrophoretic mobility, zeta potential, and fixed charge density of bovine knee chondrocytes, methylmethacrylate-sulfopropylmethacrylate, polybutylcyanoacrylate, and solid lipid nanoparticles. J. Phys. Chem. B 110, 2202–2208.

Kuo, Y.C., 2005. Loading efficiency of stavudine on polybutylcyanoacrylate and methylmethacrylate-sulfopropylmethacrylate copolymer nanoparticles. Int. J. Pharm. 290, 161–172.

Kuo, Y.C., Chung, C.Y., 2005. Transport of zidovudine- and lamivudine-loaded polybutylcyanoacrylate and methylmethacrylate-sulfopropylmethacrylate nanoparticles across the in vitro blood–brain barrier: characteristics of the drug-delivery system. J. Chin. Inst. Chem. Eng. 36, 627–638.

Lemberg, D.A., Palasanthiran, P., Goode, M., Ziegler, J.B., 2002. Tolerabilities of antiretrovirals in paediatric HIV infection. Drug Saf. 25, 973–991.

Li, X., Chan, W.K., 1999. Transport, metabolism and elimination mechanisms of anti-HIV agents. Adv. Drug Deliv. Rev. 39, 81–103.

Liend, R., Padilla, F.C., Quintana, A., 1997. Characterization of cocoa butter extracted from Criollo cultivars of *Theobroma cacao* L. Food Res. Int. 30, 727–731.

Markkanen, A., Penttinen, P., Naarala, J., Pelkonen, J., Sihvonen, A.P., Juutilainen, J., 2004. Apoptosis induced by ultraviolet radiation is enhanced by amplitude modulated radiofrequency radiation in mutant yeast cells. Bioelectromagnetics 25, 127–133.

Molla, A., Mo, H., Vasavanonda, S., Han, L., Lin, C.T., Hsu, A., Kempf, D.J., 2002. In vitro antiviral interaction of lopinavir with other protease inhibitors. Antimicrob. Agents Chemother. 46, 2249–2253.

Oscar, K.J., Hawkins, T.D., 1977. Microwave alteration of the blood–brain barrier system of rats. Brain Res. 126, 281–293.

Pang, S., Koyangi, Y., Miles, S., Wiley, C., Vinters, H.V., Chen, I.S.Y., 1990. High levels of unintegrated HIV-1 DNA in brain tissue of AIDS dementia patients. Nature 343, 85–89.

Peneafiel, L.M., Litovitz, T., Krause, D., Desta, A., Mullins, J.M., 1993. Role of modulation on the effect of microwaves on ornithine decarboxylase activity in L929 cells. Bioelectromagnetics 18, 132–141.

Poduslo, J.F., Curran, G.L., 1996. Increased permeability of superoxide dismutase at the blood–nerve and blood–brain barriers with retained enzymatic activity after covalent modification with naturally occurring polyamine, putrescine. J. Neurochem. 67, 734–741.

Quintanar-Guerrero, D., Tamayo-Esquivel, D., Ganem-Quintanar, A., Allémann, E., Doelker, E., 2005. Adaptation and optimization of the emulsification–diffusion technique to prepare lipidic nanospheres. Eur. J. Pharm. Sci. 26, 211–218.

Salford, L.G., Brun, A., Eberhardt, J.L., Persson, B.R.R., 1994. Permeability of blood–brain barrier induces by 915 MHz electromagnetic radiation, continuous wave and modulation at 8, 16, 50, and 200 Hz. J. Electroanal. Chem. 27, 535–542.

Schirmacher, A., Winters, S., Fischer, S., Goeke, J., Galla, H.J., Kullnick, U., Ringelstein, E.B., Stögbauer, F., 2000. Electromagnetic fields (1.8 GHz) increase the permeability to sucrose of the blood–brain barrier in vitro. Bioelectromagnetics 21, 338–345.

Sommerfeld, P., Schroeder, U., Sabel, B.A., 1997. Long–term stability of PBCA nanoparticle suspensions suggests clinical usefulness. Int. J. Pharm. 155, 201–207.

Strazielle, N., Ghersi-Egea, J., 2005. Factors affecting delivery of antiviral drugs to the brain. Rev. Med. Virol. 15, 105–133.

Williams, W.M., Lu, S.T., Cerro, M.D., Hoss, W., Michaelson, S.M., 1984a. Effect of 2450-MHz microwave energy on the blood–brain barrier: an overview and critique of past and present research. IEEE Trans. Microw. Theory Tech. 32, 808–818.

Williams, W.M., Hoss, W., Formaniak, M., Michaelson, S.M., 1984b. Effect of 2450-MHz microwave energy on the blood–brain barrier to hydrophilic molecules: effect on the permeability to HRP (horseradish peroxidase). Brain Res. Rev. 7, 171–181.

Yang, S.C., Lu, L.F., Cai, Y., Zhu, J.B., Liang, B.W., Yang, C.Z., 1999. Body distribution in mice of intravenously injected camptothecin solid lipid nanoparticles and targeting effect of brain. J. Control. Rel. 59, 299–307.